Robotic Batch Somatic Cell Nuclear Transfer Based on Microfluidic Groove

Yaowei Liu, *Member, IEEE*, Xuefeng Wang, *Member, IEEE*, Qili Zhao, *Member, IEEE*, Xin Zhao, *Member, IEEE*, and Mingzhu Sun, *Member, IEEE*

***Abstract*— Somatic cell nuclear transfer (SCNT), which is an important procedure in cloning, has been conducted manually for decades. The operating efficiency drops sharply in batch SCNT because of the long-time observation under microscopy and the time-wasting traditional process. Though the operating time was reduced by robotic SCNT in previous studies, the traditional operating process was still used. In this article, we designed a new robotic batch SCNT process based on a microfluidic groove and two micropipettes in parallel. By using this new SCNT process, the operating area switching, objective lens conversing, and focusing on traditional SCNT process were eliminated, and oocyte localization was simplified, which saved much operating time. Experimental results showed that the new robotic batch process reduced about 50 s (41.7%) compared with the manual process (proposed 70 s versus manual 120 s). A success rate of 93.3% ($n = 30$) and a survival rate of 96.4% were achieved ($n = 28$), which were similar to manual process. The new robotic batch SCNT method demonstrated a high degree of efficiency and reproducibility.**

***Note to Practitioners*—This article presented a new robotic somatic cell nuclear transfer (SCNT) process. This new robotic SCNT process introduced a microfluidic groove for oocyte storage and two micropipettes for oocyte enucleation and oocyte injection, respectively. We save much operating time since the operating area switching, objective lens conversing, and focusing on traditional SCNT process were eliminated, and oocyte localization was simplified. Experimental results have demonstrated the efficiency and reproducibility of the new robotic SCNT process. This new robotic SCNT process has great potential for many other applications, e.g., ICSI, embryo microinjection, and cell biopsy. Commercialization of the proposed technology may lead to the improvement in SCNT industry. In current experiments, the somatic cells sometimes were injected at the same time, which led to the failure of the experiments. In the future, we will apply control algorithms to control the motion of multiple cells.**

***Index Terms*— Micromanipulation system, microfluidic groove, robotic batch cell manipulation, somatic cell nuclear transfer (SCNT), visual detection.**

Manuscript received January 31, 2020; revised March 31, 2020; accepted April 20, 2020. Date of publication May 6, 2020; date of current version October 6, 2020. This article was recommended for publication by Associate Editor L. Zhang and Editor D. O. Popa upon evaluation of the reviewers' comments. This work was supported in part by the National Key R&D Program of China under Grant 2018YFB1304905, in part by the National Natural Science Foundation of China (NSFC) under Grant U1813210, Grant 1613220, and Grant 61903201, and in part by the Natural Science Foundation (NSF) of Tianjin under Grant 18JCYBJC19000 and Grant 18JCZDJC39100. *(Corresponding author: Mingzhu Sun.)*

The authors are with the Institute of Robotics and Automatic Information System (IRAIS), Nankai University, Tianjin 300350, China, and also with the Tianjin Key Laboratory of Intelligent Robotic (tjKLIR), Nankai University, Tianjin 300350, China (e-mail: sunmz@nankai.edu.cn).

This article has supplementary downloadable material available at http://ieeexplore.ieee.org, provided by the authors.

Color versions of one or more of the figures in this article are available online at http://ieeexplore.ieee.org.

Digital Object Identifier 10.1109/TASE.2020.2989760

I. Introduction

CLONING is a technique in which the nucleus of a somatic cell (SC) is transferred into an enucleated oocyte for the generation of a new individual by asexual reproduction. SC nuclear transfer (SCNT) is one of the main steps of cloning [1]–[4]. SCNT is a complex operating process under a microscope. Its main procedure consists of oocyte localization and holding, oocyte rotation and penetration, enucleation, SC injection, and oocyte releasing [5].

In the past two decades, SCNT has been conducted manually by highly skilled experimental operators. They dexterously controlled multiple micromanipulation devices under the eyepieces of a microscope and switched to the different operating areas six times to convert the objective lens twice and focus four times in a complete process of the nuclear transfer. The personnel factor is one of the most important factors affecting the success rate of SCNT. Moreover, as the operators need to operate multiple oocytes in one experiment, the operating efficiency drops sharply with the fatigue of the personnel after a long time of microscopic observation and repeated operation. Therefore, it is necessary to replace manual batch operations by robotic batch SCNT operation.

In the past 20 years, robotics has made great progress in cell micromanipulation, for example, robotic adherent cell injection [6], blastocyst injection [7], intracytoplasmic sperm injection [8], cell biopsy [9], [10], and so on [11]–[15]. These automation methods are effective in reducing labor intensity and improving operating efficiency. However, the operating process of SCNT is very complex; it is difficult to reduce the operating time by robotizing the manual process directly. There are two kinds of cells (oocytes and SCs) with different sizes in SCNT; the main reason for low operating efficiency is that we need to move the stage, convert, and focus the objective lens frequently for cell switching and cell localization. In previous works, we designed the global map of all operating areas and implemented a robotic batch SCNT process [16]. By using the robotic system, we did not need to convert the objective lens and reduced the focusing times of the objective lens. However, the operating time was not reduced greatly since the operating process of manual SCNT was still used. We also tried to store the oocytes in a thick pipette to simplify oocyte localization [17]. However, the number of oocytes in the pipette was limited due to the big size of the oocytes.

In traditional batch SCNT, the oocytes and cells scatter in different areas in the petri dish. It takes a long time to switch to these areas and find proper cells. Meanwhile, oocyte enucleation and SC injection share one micropipette, which makes the operation more complicated. Some researchers

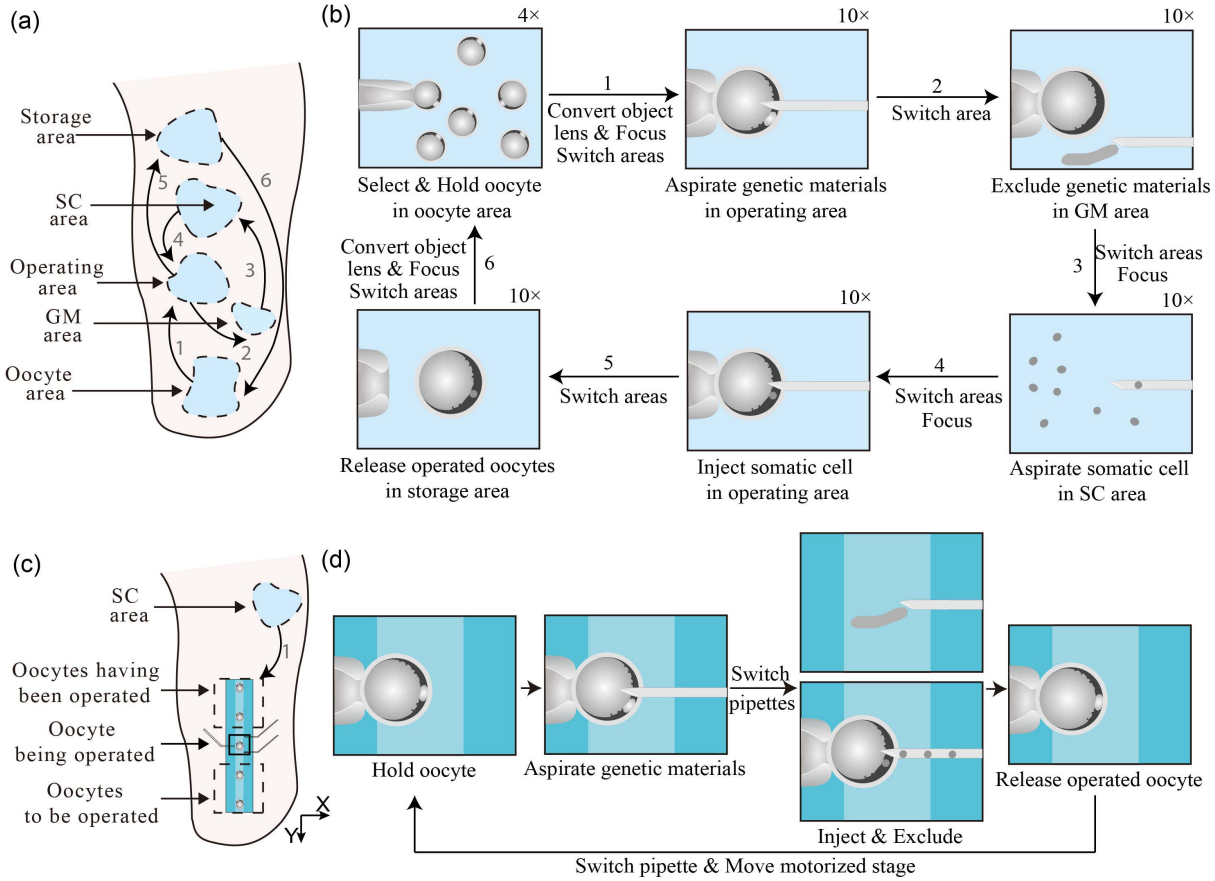

Fig. 1. Comparison between traditional robotic SCNT process and new robotic batch SCNT process. (a) Area distribution in traditional SCNT. (b) Traditional SCNT process. (c) Distribution in new robotic batch SCNT. (d) New robotic SCNT process.

conducted preliminary explorations for these problems. For example, Gibson *et al.* [18] reported a holographic assembler workstation for optical trapping and micromanipulation to arrange and hold the cells, by which they could save the time of area switching and cell holding. However, the laser confined the size of the cells in several microns in diameter. Zou *et al.* [19] designed a system that operated and located cells with an external electric field. However, it is difficult for the electric field force to overcome the penetration force. Ichikawa *et al.* [20], [21] designed and fabricated some new operating tools to fulfill the nuclear transfer process, including microgripper for oocyte holding and microknife for oocyte penetration, so that the enucleation process and injection process were separated. However, it was still a problem to rotate the cell using these tools in a closed chip. Zhang *et al.* [22] developed a robotic system for the pick-and-place of batch embryos. The throughput of this robotic system was three times that of manual operation. This method provides a good way for us to arrange the SCs.

In this article, we designed a new robotic batch SCNT process based on a microfluidic groove and two micropipettes in parallel. We first analyzed the oocyte operations in the groove by fluid theory, and then, we realized the key steps in robotic batch SCNT, including oocyte localization, oocyte holding, and double-micropipette switching. This new robotic process eliminated operating area switching, objective lens conversing, and focusing and simplified oocyte localization. The experiment results showed that the new SCNT process reduced about 50 s (41.7%) compared with the manual process.

II. Design of the New Batch Nuclear Transfer Process

A. Analysis of SCNT Process

In traditional SCNT, the oocytes and SCs are placed in the "oocyte area" and "SC area" separately in the culture medium droplet. The "operating area," "storage area," and "genetic material (GM) area" (the GM in this article means the nucleus and some cytoplasm) are also set to perform the nuclear transfer and to store the operated oocytes and the useless GMs, respectively. Fig. 1(a) shows the distribution of these areas. In one SCNT process, the oocyte is taken from the "oocyte area," operated in the "operating area," and stored in the "storage area" after nuclear transfer. The solid arrows in Fig. 1(a) show this process. During manipulation, operators aspirate the nucleus and polar body of the oocyte in "operating area," exclude the material in "GM area," aspirate the SC in "SC area," and go back to the "operating area" to inject the SC into the enucleated oocyte, as shown in the dotted arrows in Fig. 1(a). All these manipulations are performed by one injection micropipette. In the previous study, we used

the global map and a global field of view of batch oocytes to expedite SCNT, but we still needed to switch to these different areas six times for each SCNT [16].

In one traditional SCNT process, as shown in Fig. 1(b), the operators perform the nuclear transfer in the following steps.

1) Convert to 4× objective and focus, select, and hold one oocyte using the holding micropipette from the "oocyte area."
2) Convert to 10× objective and focus, rotate the oocyte, and aspirate the GMs from the oocyte to the injection micropipette in the "operating area."
3) Exclude the GMs from the injection micropipette to the "GM area."
4) Focus on the SC plane, select an SC, and aspirate it into the injection pipette from the "SC area."
5) Focus on the oocyte plane and inject the SC into the enucleated oocyte back in the "operating area."
6) Release and store the operated oocyte in the "storage area."

As shown in Fig. 1, the operators need to switch to different operating areas six times, convert the objective lens twice, and focus four times in a complete process of SCNT. In the previous study, we have used the global map to locate each operating area and a global field of view of batch oocytes for oocyte localization without objective lens conversion [16], but we still needed to switch to these different areas six times and focus the objective lens two times for SC selection in each SCNT.

There are two kinds of cells (oocytes and SCs) with different sizes and different focal planes in SCNT; we need to move the stage, convert, and focus on the objective lens frequently for cell switching and cell localization, which is the main cause of the tedious operating process.

In this article, we improved the SCNT process in two ways. On one hand, we placed the oocytes in a microfluidic groove in one dimension along the Y-axis, as shown in Fig. 1(c). It was easy to distinguish the operated oocytes and the oocytes to be operated so that oocyte localization could be simplified, and "oocyte area" and "storage area" in Fig. 1(a) were removed. On the other hand, two micropipettes in parallel were introduced in robotic batch SCNT for oocyte enucleation and SC injection, respectively. Multiple SCs were aspirated in the injection micropipette before the SCNT process; we only switched to the "SC area" and focused when all SCs in the injection micropipette were used. Meanwhile, SC injection by injection micropipette could be synchronized with GM exclusion by enucleation micropipette so that the "GM area" was also removed. Fig. 1(d) shows the improved SCNT process; we only needed to switch the micropipettes twice and move the motorized stage once along Y-axis, which simplified the operating process greatly.

B. Process of Robotic Batch SCNT

Based on the previous analysis, we designed the new batch SCNT process, as shown in Fig. 2. The detailed steps are listed as follows.

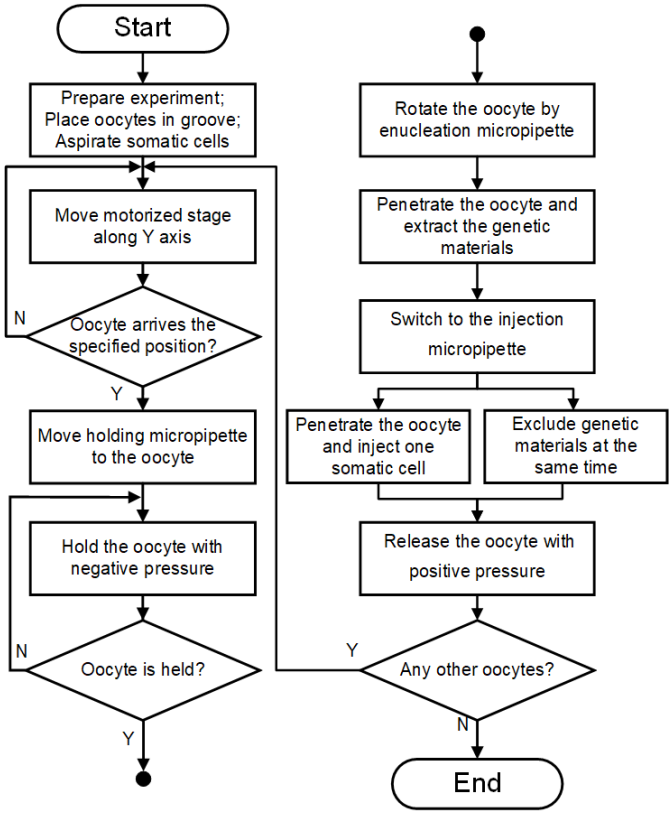

Fig. 2. Robotic batch SCNT process scheme.

1) Prepare the experiments. Place the oocytes in the groove. Aspirate multiple SCs in the injection micropipette.
2) Drive the electric stage to move along the Y-axis until the oocyte to be operated appears in the microscopic field. Move this oocyte to the center of the field of view.
3) Move the holding micropipette along the X-axis to the oocyte. Hold the oocyte with negative pressure by the pressure controller.
4) Move the enucleation micropipette along the X-axis to approach the oocyte. Rotate the oocyte by the enucleation micropipette until the polar body is pointed to the desired position for enucleation [23].
5) Penetrate the oocyte and extract the GMs from the oocyte by the enucleation micropipette and then withdraw the enucleation micropipette.
6) Move the enucleation micropipette along the Y-axis until the injection micropipette appears in the microscopic field.
7) Penetrate the oocyte by the injection micropipette through the wound leaving by enucleation and inject one SC into the oocyte [22]. Meanwhile, exclude the GMs from the enucleation micropipette out of the microscopic field. Withdraw the injection micropipette.
8) Release the operated oocyte with positive pressure.
9) Repeat steps 2–8 if there are oocytes to be operated; otherwise, end the whole operation.

In the new batch SCNT process, the oocytes were placed in the groove and close to each other. Oocyte holding operations may cause unnecessary interference with the surrounding

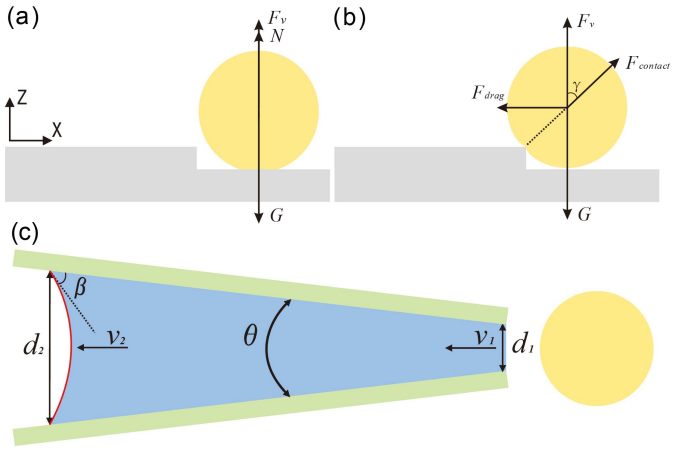

Fig. 3. Calculation of the minimum holding pressure. (a) Force analysis in the groove. (b) Minimum dragging force analysis. (c) Fluid flow near the micropipette.

oocytes by the movement of the culture medium. In order to aspirate one and only one oocyte from the groove, we first analyzed the force of the oocyte in the groove by fluid theory and calculated the minimum pressure for oocyte holding. Then, we focused on the realization of the key steps in robotic batch SCNT, including oocyte localization in step 2, oocyte holding in step 3, and micropipettes switching in step 6. Robotic oocyte rotation in step 4 and multiple-SC injection in step 7 were realized by the methods in [23] and [22], respectively. In step 5, the endpoint of enucleation was determined by human–computer interaction due to the difficulty of visual detection.

III. Key Method of Robotic Batch SCNT

A. Minimum Holding Pressure Calculation

As the oocytes are approximately sphere, we analyzed the force assuming the oocyte as a uniform sphere in this article.

According to the law of Newtonian mechanics [as shown in Fig. 3(a)], when the oocytes are at the bottom of the groove, we have

$$N = G - F_v = \frac{4}{3}(\rho_{\text{cell}} - \rho_{\text{fluid}})\pi R^3 g \tag{1}$$

where N is the bracing force of the bottom, G is the gravity, F_v is the buoyancy force, R is the radius of the cell, g is the gravitational acceleration, ρ_{fluid} is the density of the fluid, and ρ_{cell} is the density of the cell.

When the holding micropipette starts to aspirate the oocyte, the cell is affected by the dragging force F_{drag}, which is generated by the fluidic flow. With the increase in F_{drag}, the cell contacts with the upper edge of the groove. Then, the contact force F_{contact} is generated, as shown in Fig. 3(b). In the vertical direction, the Z-component of F_{contact} cancels out the bracing force N gradually. The acceleration of the oocyte can be regarded as zero when the bracing force just disappears. Analyzing the force balance state, the following equation can be obtained:

$$G - F_v = F_{\text{contact}} \cos\gamma \tag{2}$$

$$F_{\text{drag}} = F_{\text{contact}} \sin\gamma \tag{3}$$

where γ is the angle between the direction of the contact force and the vertical direction. Then, the dragging force F_{drag} can be calculated by (3).

The dragging force caused by the fluid flow F_{drag} can be calculated as

$$F_{\text{drag}} = \frac{1}{2}\rho_{\text{fluid}} V^2 C_D A \tag{4}$$

where V is the velocity of the fluid near the oocyte, C_D is the drag coefficient of an oocyte, and A is the cross-sectional area of the micropipette outlet. In the experiments, the outlet of the holding micropipette is close to the oocyte. Accordingly, the fluid velocity near the cell V can be considered the same as the fluid velocity at the outlet of the holding micropipette v_1 ($V \approx v_1$).

According to the continuum model of the fluid, we have

$$\rho_{\text{fluid}} v_1 A_1 = \rho_{\text{fluid}} v_2 A_2 \tag{5}$$

where A_1 and A_2 are the cross-sectional area of the micropipette outlet and gas–liquid interface (GLI) [the red curve in Fig. 3(c)] and v_2 is the fluid velocity of the GLI. The relationship between the fluid velocity of the micropipette outlet v_1 and the GLI v_2 can be obtained by (5)

$$v_2 = \left(\frac{d_2}{d_1}\right)^2 v_1 \tag{6}$$

where d_1 and d_2 are the diameters of the micropipette outlet and the GLI.

Because the fluid is incompressible and viscous effects can be ignored in the experiments, according to the Bernoulli equation, we have

$$z_1 + \frac{P_1}{\rho_{\text{fluid}} g} + \frac{{v_1}^2}{2g} = z_2 + \frac{P_2}{\rho_{\text{fluid}} g} + \frac{{v_2}^2}{2g} + \xi_D \frac{{v_2}^2}{2g} \tag{7}$$

where z_1 and z_2 are the altitudes of the micropipette outlet and the GLI, P_1 and P_2 are the pressures of the micropipette outlet and the GLI, and ξ_D is the loss factor. As the end of the micropipette is placed horizontally, we have $z_1 = z_2$. Then, the relationship between the fluid velocity of the micropipette outlet v_1 and the pressure difference $\Delta P = P_2 - P_1$ can be obtained

$$\Delta P = \frac{1}{2}\rho_{\text{fluid}}\left(1 - (1 + \xi_D)\left(\frac{d_2}{d_1}\right)^4\right){v_1}^2. \tag{8}$$

Because the shape of holding micropipette is narrow in the front and wide in the back [as shown in Fig. 3(c)], the loss factor ξ_D contains the friction coefficient of micropipette wall ξ_{TP} and the coefficient of expansion resistance ξ_{pacm}

$$\xi_D = \xi_{\text{TP}} + \xi_{\text{pacm}}. \tag{9}$$

ξ_{TP} can be calculated by

$$\xi_{\text{TP}} = \frac{\lambda}{8\sin\theta/2}\left[1 - \left(\frac{A_1}{A_2}\right)^2\right] \tag{10}$$

where λ is the friction coefficient of the fluid and θ is the diffusion angle of the micropipette [as shown in Fig. 3(c)].

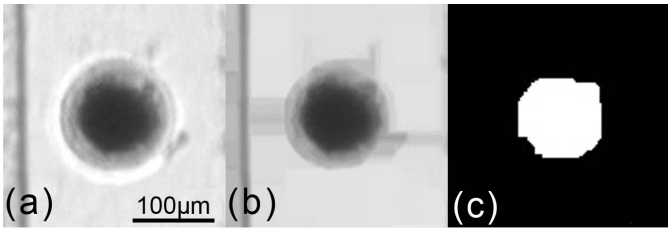

Fig. 4. Process of oocyte position detection. (a) Original image. (b) Image after morphological opening. (c) Binary image created by OTSU adaptive thresholding.

The fluid flow in the micropipette can be considered as laminar, and λ is the function of the Reynolds number R_e

$$\lambda = \frac{64}{R_e} = \frac{64\mu}{\rho_{\text{fluid}} v_1 d_1} \tag{11}$$

where μ is the viscosity coefficient of the fluid.

When the diffusion angle is between 0° and 40°, the coefficient of expansion resistance ξ_{pacm} can be empirically correlated as

$$\xi_{\text{pacm}} = 3.2 \tan \frac{\theta}{2} \sqrt{[4]\tan \theta/2 \left[1 - \left(\frac{A_1}{A_2}\right)^2\right]}. \tag{12}$$

The Bernoulli equation describes the energy conservation of the macroscopic fluids. The surface tension is an important factor in microfluidics, so (8) is modified as [24]

$$\Delta P = \frac{1}{2}\rho_{\text{fluid}}\left(1 - (1 + \xi_D)\left(\frac{d_2}{d_1}\right)^4\right){v_1}^2 + \frac{4\sigma \cos \beta}{d_2} \tag{13}$$

where σ is the surface tension coefficient of the fluid and β is the contact angle between the fluid and the air [as shown in Fig. 3(c)].

B. Oocyte Localization

When the electric stage moved along the Y-axis, the oocyte would appear in the microscopic field. We detected the oocyte according to the shape and contrast of the oocyte in microscopic images. We focused on two parameters of the oocyte: the area A_{oocyte} and the roundness C_l. The morphological filters were used to get the parameters in this article. First, the morphological opening was used to remove the noise of small particles and extrude the edge in the original image, as shown in Fig. 4(b). Second, the binary image was obtained by using the OTSU adaptive threshold algorithm, as shown in Fig. 4(c), so that the foreground was separated from the background.

We got the position of the oocyte by the following steps.

1) Calculate the values of A_{oocyte} and C_l. The oocyte area A_{oocyte} was calculated by counting up all the white pixels in Fig. 4(c). The roundness C_l was defined as

$$C_l = \frac{4\pi A_{\text{oocyte}}}{{L_{\text{oocyte}}}^2} \tag{14}$$

where L_{oocyte} was the perimeter of the binary image of the oocyte.

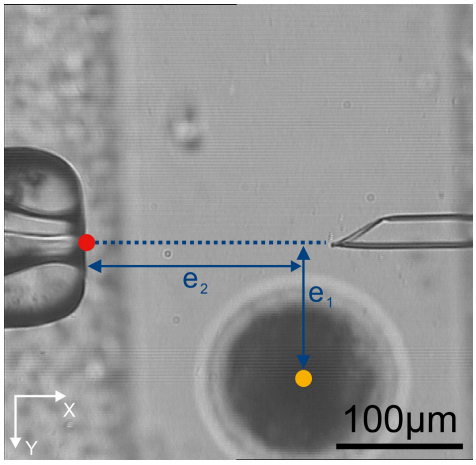

Fig. 5. Oocyte localization.

2) Remove unnecessary objects by setting a reasonable roundness threshold (the threshold is 0.64 in this article).
3) Obtain the position of the oocyte to be operated. If there were multiple oocytes in the field of view, the oocytes were sorted using the bubble sort method to find the nearest oocyte to the holding micropipette.

Now, we knew the position of the oocyte to be operated (the orange point in Fig. 5) and the position of the holding micropipette (the red point in Fig. 5), which was detected by the template matching method. The red point was also the endpoint of the oocyte movement. We could calculate the vertical distance between the holding micropipette and oocyte (e_1) and the horizontal distance between the holding micropipette and oocyte (e_2). e_1 and e_2 were set as the inputs of the motorized stage and holding micropipette manipulator. The motorized stage moved the distance of e_1 along the Y-axis and the holding manipulator moved the distance of $e_2 - R_{\text{oocyte}}$ along the X-axis so that the holding micropipette was close to the oocyte.

C. Oocyte Holding

We used the sharpness of the oocyte to determine whether the oocyte left the groove and was held by the holding micropipette. The clarity evaluation method was applied to measure the sharpness of the oocyte in the image. The evaluation function was defined by the normalized variance

$$F = \frac{1}{M \times N \times \varepsilon} \sum_{i=1}^{M} \sum_{j=1}^{N} [I(i, j) - \varepsilon]^2 \tag{15}$$

where M and N were the height and width of the image, respectively, $I(i, j)$ was the pixel intensity at (i, j), and ε was the average intensity. Compared with the other clarity evaluation method [25], the normalized variance method provided a unimodal curve of the sharpness of the oocyte so that the focusing of the oocyte could be clearly distinguished.

The oocyte was held by the following steps. First, the region of interest (ROI) of the oocyte was obtained; both the holding micropipette outlet and the oocyte were visible in the ROI. Second, the pneumatic syringe provided a negative pressure,

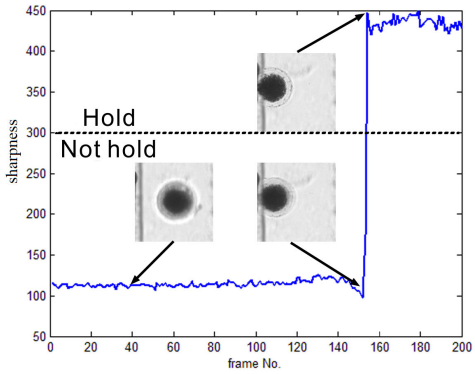

Fig. 6. Sharpness of the ROI image for cell holding state detection.

which was slightly larger than the minimum pressure to drag the oocyte. At the same time, the values of the evaluation function were calculated in the ROI image continuously. The cell holding state was easily distinguished by comparing the sharpness difference of the image with a reasonable threshold (as shown in Fig. 6). Finally, we confirmed that the oocyte has been held and started rotating oocyte.

D. Function Switching of Enucleation and Injection

The enucleation micropipette and injection micropipette were held in parallel in the same micromanipulator during the experiments. However, there was only one micropipette appears in ten times microscopic field [see Fig. 7(a)]. Therefore, we needed to design a fast switching method to improve the operating efficiency in the process of switching between the enucleation and SC injection. Meanwhile, we must ensure that the injection micropipette penetrated the oocyte again from the wound (caused by enucleation) after switching; otherwise, the injection micropipette would penetrate the oocyte from other positions. In that case, the cytoplasm would flow from the original wound, making the experiment fail.

The relative position between the enucleation micropipette and injection micropipette would not change in the experiments, as shown in Fig. 7(b). Therefore, we first calibrated the rough distance between the two micropipettes (D_{rough}) under four times the objective lens before experiments. Second, we recorded the positions of the enucleation micropipette or injection micropipette by template matching algorithm under ten times an objective lens. When the two micropipettes needed to be switched in the experiments, the current micropipette moved the distance D_{rough} along the Y-axis so that another micropipette would quickly appear in the field of view.

Finally, we relocated the current micropipette to the desired position, which was convenient for oocyte penetration; 15 oocytes were used to verify the accuracy of micropipettes switching. The results showed that the success rate was 100%.

IV. Experiments and Results

A. System Design

Micromanipulation system consists of the following parts [see Fig. 8(a) and (b)]: a standard inverted microscope

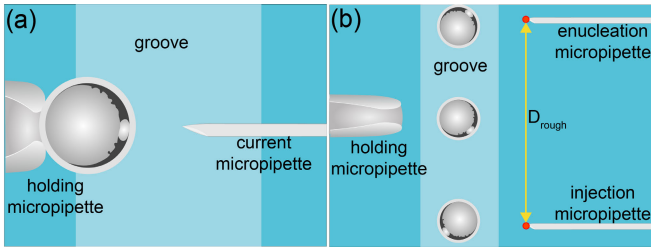

Fig. 7. (a) Schematic under ten times microscopic field. (b) Rough distance between the enucleation micropipette and the injection micropipette under four times microscopic field.

(Olympus, BX-51, Japan) as the basic platform of the system, a pair of in-house developed motorized X-Y-Z micromanipulators (range of movement: 50 mm × 50 mm × 50 mm, repeatability: 1 μm, and maximum speed: 1 mm/s), an in-house developed motorized X-Y stage (range of movement: 100 mm × 100 mm, repeatability: 1 μm, and maximum speed: 2 mm/s), a CCD camera (Panasonic, W-V-460, Japan), three micropipette holders (Narishige, HI-7, Japan), a double pipette holder (Narshige, HD-21, Japan), a self-developed syringe (including the motor controller, Zolix, ASM-XYZ-1A, China) based on pressure accumulation principle, a pressure controller box based on pneumatic principle, a host computer for pressure data acquisition, image processing, and motion control [23], [26], [27].

The groove was made up of polymethyl methacrylate (PMMA). It is easy to fabricate a large channel with a wide width ratio and good light transmittance without biological toxicity by PMMA. In this article, the surface of the groove was treated with hydrophilicity. In order to prevent the porcine oocytes from being trapped by the microgroove, we designed the microgroove as follows: the width was greater than the diameter of the oocytes, and the depth was a little less than the radius of the oocytes. In this article, the width and depth of the groove were set to 60 and 250μm, respectively. The oocytes were manually placed in the groove by the operators before the experiments. Since it is not necessary to place the cells at a precise point, this operation does not increase the complexity of the experiments. The groove is a nonclosed structure so that it does not bother with the subsequent operations.

The two micropipettes for enucleation and injection were fixed by a double pipette holder (see Fig. 9). The enucleation micropipette (the upper micropipette) was used to extract the GMs from the oocyte. The injection micropipette (the lower micropipette) was used to inject the SC into the enucleated oocyte. The holding micropipette and the enucleation micropipette were connected to the "pressure controller." The injection micropipette was connected to the "motorized syringe" [see Fig. 8(a)].

B. Minimum Holding Pressure

In this article, we used the porcine oocyte in the experiments. The radius and the density of the oocyte are 75 ± 5 μm and 1049.5 ± 9.2 kg/m^3, respectively [24]. The density of the culture medium is approximately 1008.2 kg/m^3 [24]. In (1), the bracing force of the bottom N is 4.5–10.6 × 10^{-10} N.

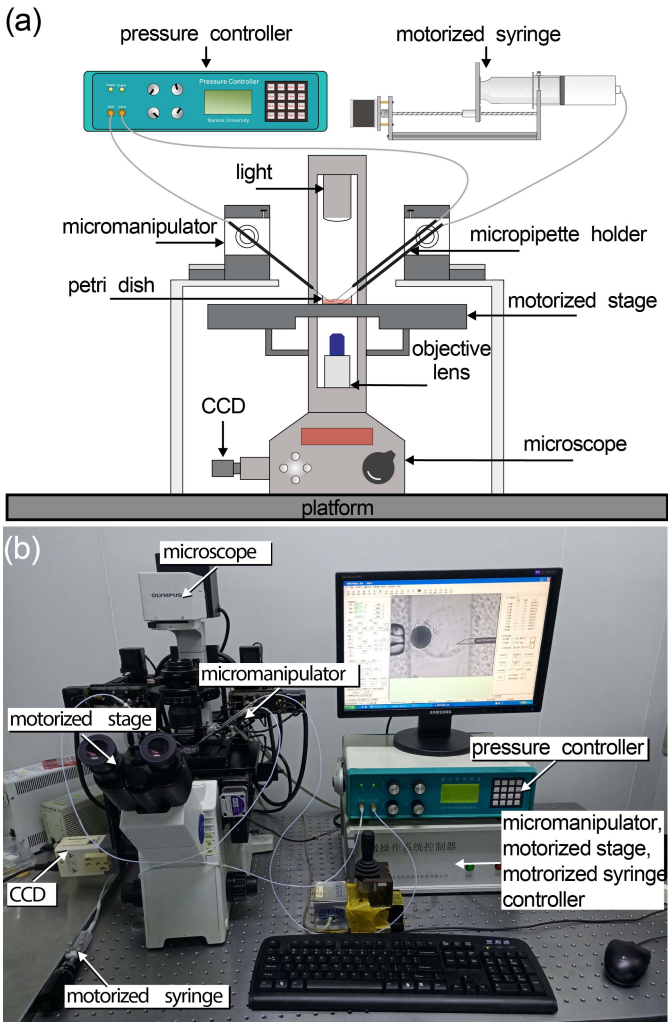

Fig. 8. (a) Schematic of the robotic batch SCNT system. (b) Robotic batch SCNT system setup.

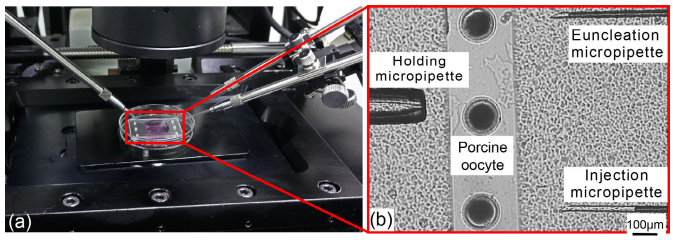

Fig. 9. Two micropipettes for enucleation and injection. (a) Experimental image shows the two micropipettes for enucleation and injection. (b) Experimental image shows the two micropipettes for enucleation and injection under four times microscopic field.

The depth of the groove is 60 μm, and γ is approximately 11.5°, as shown in Fig. 3(b). In (2) and (3), the minimum dragging force from the fluid flow F_{drag} is about 0.9–2.1 $\times$ 10^{-10} N.

The dragging coefficient of a sphere oocyte equals to 0.47 [28]. In (4), the fluid velocity (V) that generates the sufficient force to drag the oocyte can be calculated to be 0.017–0.026 m/s. $\sin\theta/2$ is 0.02, A_1/A_2 is 0.857, the viscosity coefficient of fluid is $1656.9\times10^{-6}\text{m}^2/\text{s}$ [29], d_1 is 50 μm, and d_2 is 54 μm. In (9)–(12), the loss factor ξ_D can be calculated to be 119.2. $R_H = d_1/2 = 25$ μm. Therefore, in (13), the minimum holding pressure P could be calculated as 1706.2–1737.9 Pa. In the experiments, the pressure to hold the oocyte was set as 1750 Pa (a little bigger than the calculated results) to ensure the success of oocyte holding. We did the aspiration experiment with the pressure of 1750 Pa. Because the density of the culture medium would change with time and environment temperature, we did the SCNT experiment of each batch in 15 min and changed the culture medium for the next batch experiment. In the experiment, the distance between the adjacent oocytes was about 200–220 μm. The experimental results showed that the success rate of oocyte holding was 100% ($n = 20$), and the other oocytes did not move when the target oocyte was held.

TABLE I
OOCYTE POSITION DETECTION AND OOCYTE HOLDING DETECTION

Method	Number	Threshold	Success Rate
Oocyte Position	30 oocytes	0.64	96%(29/30)
Oocyte Holding	30 oocytes	400	100%(30/30)

C. Experimental Process and Results

1) Visual Detection Results of Oocyte Position and Holding: Thirty oocytes were used to verify the oocyte position algorithm and oocyte holding algorithm. As shown in Table I, The success rate of oocyte position detection was 96%, and the success rate of oocyte holding detection was 100%. The threshold of roundness C_l in the oocyte position algorithm was set as 0.64, and the threshold of evaluation value in the oocyte holding algorithm was set as 400. Oocyte position detection failed when the impurity in the culture medium contacted with oocytes, which changed the outline of the oocytes.

2) Micropipette Switching Results: Fifteen oocytes were used to verify the accuracy of micropipettes switching. The distance between the two micropipettes in parallel was 790 μm. Each oocyte was first penetrated and enucleated by the enucleation micropipette and then injected the SC by the injection micropipette. It took about 7 s to switch the micropipette and relocate the current micropipette. The experimental results showed that the success rate was 100%.

3) SCNT Operating Results: In this article, we used the porcine oocytes and porcine fetal fibroblasts as oocytes and SCs. We operated three batches of ten oocytes by the proposed new robotic SCNT, and the typical operating process is shown in Fig. 10. Fig. 10(a) shows the state of locating and holding the oocyte; Fig. 10(b) shows the state of rotating the oocyte to the desired orientation; Fig. 10(c) shows the state of aspirating the GMs from the oocyte; Fig. 10(d) shows the state of switching the enucleation and injection micropipette; Fig. 10(e) shows the state of preparing for injection; Fig. 10(f) shows the state of injecting the SC into the enucleated oocyte; Fig. 10(g) shows the state of switching the enucleation micropipette back; and Fig. 10(h) shows the state of releasing the oocyte and finding the next oocyte. Video (Movie.avi) given in the

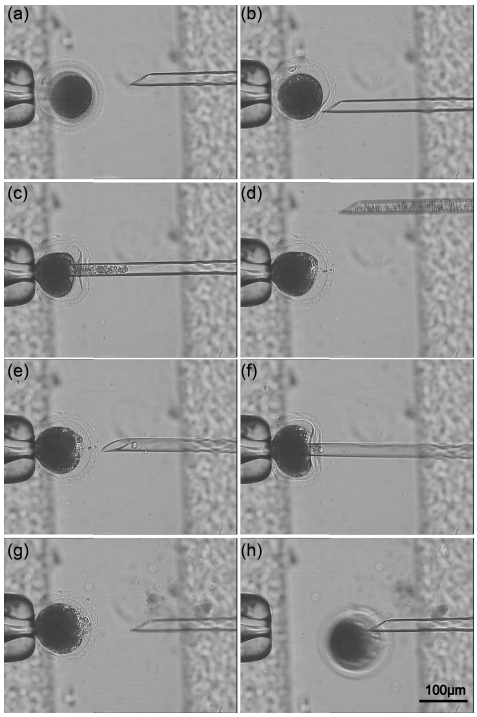

Fig. 10. Typical operating process. (a) Locate and hold the oocyte. (b) Rotate the oocyte. (c) Aspirate the GMs from the oocyte. (d) Switch the injection micropipette. (e) Prepare to inject. (f) Inject the SC. (g) Switch the enucleation micropipette back. (h) Release the operated oocyte.

Supplementary Material shows the operating process of the proposed method.

The average costing time of the proposed new robotic SCNT was 70 s, including the time for collecting SCs into the injection micropipette. While the average costing time of 30 cases of manual SCNT was 120 s and that of traditional robotic SCNT was 107 s, including the time of global map construction. Table II shows the average costing time of each step in the SCNT process. In oocyte localization, the oocytes were regularly placed in the groove before experiments in the proposed SCNT process. We only needed to search and localize the oocyte in one dimension, which saved about 10 s compared with the traditional robotic SCNT process. In SC injection, two micropipettes were used for enucleation and injection separately, and multiple SCs were aspirated in the injection micropipette before experiments. We saved the time of operating area switching for GM's exclusion and SC aspiration, so the costing time of this step was reduced from 43 to 16 s. The new robotic process reduced about 50 s (41.7%) compared with the manual process (proposed 70 s versus manual 120 s) and 37 s (34.6%) compared with the traditional robotic process (proposed new robotic 70 s versus traditional robotic 107 s).

An operation was considered successful when the robotic system achieved all steps of SCNT and successfully released the oocytes after transplantation on the microfluidic groove. Table III shows the success rates of the three kinds of operating processes. In the proposed new robotic SCNT, 28 oocytes were enucleated and injected with the SCs successfully, achieving

TABLE II

SCNT SPEED COMPARISON BETWEEN MANUAL, TRADITIONAL ROBOTIC AND NEW ROBOTIC METHODS

Methods	Manual	Traditional Robotic	New Robotic
Initialization(s)		1	1
Localization(s)		19	9
Holding(s)		2	2
Rotation(s)	N/A	26	26
Enucleation(s)		9	9
Injection(s)		43	16
Release(s)		7	7
Total(s)	120	107	70

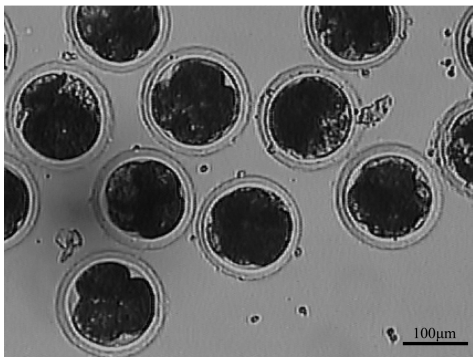

Fig. 11. Embryos after SCNT, activation, and cultured for one day.

TABLE III

SUCCESS RATE AND SURVIVAL RATE AFTER SCNT

SCNT Methods	Manual	Traditional Robotic	New Robotic
Operated oocytes	30	30	30
Success Rate	96.6%(29/30)	93.3%(28/30)	93.3%(28/30)
Survival Rate	96.5%(28/29)	96.4%(27/28)	96.4%(27/28)

a success rate of 93.3%. The failure cases occurred when two SCs in the pipette were injected into the oocyte at the same time. The proposed method greatly improved the operating efficiency with the similar success rate of the previous methods (manual: 96.6%; traditional robotic: 93.3%).

4) Embryo Culture Results After SCNT:

After SCNT, the successfully operated oocytes, which were embryos then, were first activated and then cultured at 37 °C with 5% CO_2. The experimental results are summarized in Table III. In proposed new robotic SCNT, 27 embryos were alive after one-day culture ($n = 28$), as shown in Fig. 11, achieving a survival rate of 96.4%, which was similar to that of the previous methods (manual: 96.5%; traditional robotic: 96.4%). The high survival rate demonstrates that the proposed new robotic SCNT did not cause significant damage to oocyte development.

V. CONCLUSION

SCNT is an important procedure in cloning. As a complex operating process under a microscope, SCNT has been conducted manually for decades. However, the operating efficiency drops sharply in manual SCNT due to the fatigue of the personnel. In this article, we designed a new robotic

batch SCNT process to replace the manual operation. First, a microfluidic groove and two micropipettes in parallel, which were used to replace the injection micropipette, were introduced to improve the micromanipulation system. The batch oocytes were placed in the groove, and multiple SCs were aspirated in one of the parallel micropipettes before the SCNT experiments. Second, we analyzed the force of the oocyte in the groove by fluid theory to verify the feasibility of the groove and then calculated the minimum pressure for oocyte holding. Finally, we realized the whole robotic batch SCNT process based on visual detection and motion control.

This new robotic process eliminated the operating area switching, the objective lens conversing, and focusing and simplified oocyte localization. Experimental results showed that the new robotic batch process reduced about 50 s (41.7%)/37 s (34.6%) compared with the manual process/traditional robotic process (new robotic: 70 s, traditional robotic: 107 s, and manual: 120 s). A success rate of 93.3% ($n = 30$) and a survival rate of 96.4% were achieved ($n = 28$), which were similar to manual process and traditional robotic process. The new robotic batch SCNT method demonstrated a high degree of efficiency and reproducibility.

The new batch robotic process has great potential for many other applications, e.g., ICSI, and embryo microinjection. Commercialization of the proposed technology may lead to the improvement in SCNT industry.

In the robotic batch SCNT experiments, somatic injection is the most difficult part; since there were many SCs in the injection micropipette, only one cell should be injected into the oocyte each time. In current experiments, the SCs, sometimes, stuck together with the fluid movement in the injection pipette, so two SCs sometimes were injected at the same time, which led to the failure of the experiments. In the future, we will apply solution flow modeling, balance pressure modeling, and adaptive control to control the motion of multiple cells.

REFERENCES

[1] I. Wilmut *et al.*, "Somatic cell nuclear transfer," *Nature*, vol. 419, no. 6907, pp. 583–586, 2002.

[2] K. H. S. Campbell, J. McWhir, W. A. Ritchie, and I. Wilmut, "Sheep cloned by nuclear transfer from a cultured cell line," *Nature*, vol. 380, no. 6569, pp. 64–66, Mar. 1996.

[3] H. Kuwayama, Y. Tanabe, T. Wakayama, and S. Kishigami, "Birth of cloned mice from vaginal smear cells after somatic cell nuclear transfer," *Theriogenology*, vol. 94, pp. 79–85, May 2017.

[4] S. Lee, M. Zhao, J. No, Y. Nam, G.-S. Im, and T.-Y. Hur, "Dog cloning with *in vivo* matured oocytes obtained using electric chemiluminescence immunoassay-predicted ovulation method," *PLoS ONE*, vol. 12, no. 3, 2017, Art. no. e0173735.

[5] Y. Tsunoda and Y. Kato, "The recent progress on nuclear transfer in mammals," *Zool. Sci.*, vol. 17, no. 9, pp. 1177–1184, Dec. 2000.

[6] J. Liu *et al.*, "Robotic adherent cell injection for characterizing cell–cell communication," *IEEE Trans. Biomed. Eng.*, vol. 62, no. 1, pp. 119–125, Jan. 2015.

[7] L. S. Mattos, E. Grant, R. Thresher, and K. Kluckman, "Blastocyst microinjection automation," *IEEE Trans. Inf. Technol. Biomed.*, vol. 13, no. 5, pp. 822–831, Sep. 2009.

[8] Z. Lu, X. Zhang, C. Leung, N. Esfandiari, R. F. Casper, and S. Yu, "Robotic ICSI (intracytoplasmic sperm injection)," *IEEE Trans. Biomed. Eng.*, vol. 58, no. 7, pp. 2102–2108, Jul. 2011.

[9] A. Shakoor, T. Luo, S. Chen, M. Xie, J. K. Mills, and D. Sun, "A high-precision robot-aided single-cell biopsy system," in *Proc. IEEE Int. Conf. Robot. Autom. (ICRA)*, May 2017, pp. 5397–5402.

[10] A. Shakoor *et al.*, "Achieving automated organelle biopsy on small single cells using a cell surgery robotic system," *IEEE Trans. Biomed. Eng.*, vol. 66, no. 8, pp. 2210–2222, Aug. 2019.

[11] Y. Sun and B. J. Nelson, "Biological cell injection using an autonomous microrobotic system," *Int. J. Robot. Res.*, vol. 21, nos. 10–11, pp. 861–868, Oct. 2002.

[12] W. Wang, X. Liu, D. Gelinas, B. Ciruna, and Y. Sun, "A fully automated robotic system for microinjection of zebrafish embryos," *PLoS ONE*, vol. 2, no. 9, p. e862, 2007.

[13] H. B. Huang, D. Sun, J. K. Mills, and S. Han Cheng, "Robotic cell injection system with position and force control: Toward automatic batch biomanipulation," *IEEE Trans. Robot.*, vol. 25, no. 3, pp. 727–737, Jun. 2009.

[14] Y. Xie, D. Sun, C. Liu, H. Y. Tse, and S. H. Cheng, "A force control approach to a robot-assisted cell microinjection system," *Int. J. Robot. Res.*, vol. 29, no. 9, pp. 1222–1232, Aug. 2010.

[15] Q. Xu, *Micromachines for Biological Micromanipulation*. Springer, 2018, pp. 15–47, doi: 10.1007/978-3-319-74621-0.

[16] Q. Zhao, M. Cui, X. Zhao, M. Sun, Y. Wang, and J. Feng, "Batch-operation process of nuclear transplantation based on global field of view," in *Proc. 30th Chin. Control Conf.*, Jul. 2011, pp. 4089–4094.

[17] X. Wang, N. Li, Y. Liu, M. Sun, and X. Zhao, "Pipelined batch-operation process of nuclear transplantation based on micro-manipulation system," in *Proc. IEEE Int. Conf. Robot. Biomimetics (ROBIO)*, Dec. 2016, pp. 1372–1376.

[18] G. Gibson *et al.*, "Holographic assembly workstation for optical manipulation," *J. Opt. A, Pure Appl. Opt.*, vol. 10, no. 4, Apr. 2008, Art. no. 044009.

[19] Z. Zou, S. Lee, and C. H. Ahn, "A polymer microfluidic chip with interdigitated electrodes arrays for simultaneous dielectrophoretic manipulation and impedimetric detection of microparticles," *IEEE Sensors J.*, vol. 8, no. 5, pp. 527–535, May 2008.

[20] A. Ichikawa, T. Tanikawa, K. Matsukawa, S. Takahashi, and K. Ohba, "Fluorescent monitoring using microfluidics chip and development of syringe pump for automation of enucleation to automate cloning," in *Proc. IEEE Int. Conf. Robot. Autom.*, May 2009, pp. 2231–2236.

[21] A. Ichikawa *et al.*, "On-chip enucleation of an oocyte by untethered microrobots," *J. Micromech. Microeng.*, vol. 24, no. 9, Sep. 2014, Art. no. 095004.

[22] Z. Zhang *et al.*, "Robotic pick-and-place of multiple embryos for vitrification," *IEEE Robot. Autom. Lett.*, vol. 2, no. 2, pp. 570–576, Apr. 2017.

[23] C. Zhao, Y. Liu, M. Sun, and X. Zhao, "Robotic cell rotation based on optimal poking direction," *Micromachines*, vol. 9, no. 4, p. 141, 2018.

[24] Q. Zhao, B. Shirinzadeh, M. Cui, M. Sun, Y. Liu, and X. Zhao, "A novel cell weighing method based on the minimum immobilization pressure for biological applications," *J. Appl. Phys.*, vol. 118, no. 4, Jul. 2015, Art. no. 044301.

[25] Z. Wang, C. Feng, W. T. Ang, S. Y. M. Tan, and W. T. Latt, "Autofocusing and polar body detection in automated cell manipulation," *IEEE Trans. Biomed. Eng.*, vol. 64, no. 5, pp. 1099–1105, May 2017.

[26] X. Wang, Y. Liu, S. Li, M. Cui, M. Sun, and X. Zhao, "Automated cell transportation for batch-cell manipulation," in *Proc. IEEE/RSJ Int. Conf. Intell. Robots Syst. (IROS)*, Sep. 2017, pp. 2974–2979.

[27] Q. Zhao, M. Sun, M. Cui, J. Yu, Y. Qin, and X. Zhao, "Robotic cell rotation based on the minimum rotation force," *IEEE Trans. Autom. Sci. Eng.*, vol. 12, no. 4, pp. 1504–1515, Oct. 2015.

[28] Z. Wang, C. Feng, R. Muruganandam, W. T. Ang, S. Y. M. Tan, and W. T. Latt, "Three-dimensional cell rotation with fluidic flow-controlled cell manipulating device," *IEEE/ASME Trans. Mechatronics*, vol. 21, no. 4, pp. 1995–2003, Aug. 2016.

[29] Q. Zhao, M. Sun, M. Cui, J. Yu, and X. Zhao, "Robotic weighing for spherical cells based on falling speed detection," in *Proc. Int. Conf. Manipulation, Manuf. Meas. Nanosc.*, Aug. 2013, pp. 264–268.

Yaowei Liu (Member, IEEE) received the B.Eng. degree in automation and the Ph.D. degree in control theory and control engineering from Nankai University, Tianjin, China, in 2013 and 2019, respectively.

He is currently a Post-Doctoral Fellow with the College of Artificial Intelligence, Nankai University. His research interests include micromanipulators and microsystems.

Xuefeng Wang (Member, IEEE) received the B.Eng. degree in automation from the Taiyuan University of Technology, Taiyuan, China, in 2015, and the M.S. degree in control science and engineering from Nankai University, Tianjin, China, in 2018.

His research interests include micromanipulators, microsystems, and computer vision.

Qili Zhao (Member, IEEE) received the B.Eng. degree in automation from the Shandong University of Science and Technology, Qingdao, China, in 2008, and the Ph.D. degree in control theory and control engineering from Nankai University, Tianjin, China, in 2014.

He finished his first post-doctoral research with the Robotics and Mechatronics Research Laboratory, Department of Mechanical and Aerospace Engineering, Monash University, Melbourne, VIC, Australia, in 2015. He was a Post-Doctoral Fellow with the Advanced Micro and Nanosystems Laboratory, Department of Mechanical and Industrial Engineering, Toronto University, Toronto, ON, Canada, from 2015 to 2018. He is currently an Assistant Professor with the College of Artificial Intelligence, Nankai University. His research interests include automated drug screen, robotic beating heart cells manipulation system, robotic cell manipulation, and robotic cell measurement.

Xin Zhao (Member, IEEE) received the B.S. degree from Nankai University, Tianjin, China, in 1991, the M.S. degree from the Shenyang Institute of Automation, CAS, Shenyang, China, in 1994, and the Ph.D. degree from Nankai University in 1997, all in control theory and control engineering.

He joined the faculty at Nankai University in 1997, where he is currently a Professor and the Vice Dean of the College of Artificial Intelligence. His research interests are in micromanipulator, microsystems, and mathematical biology.

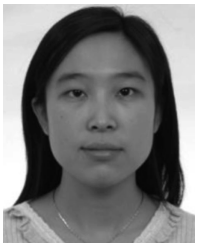

Mingzhu Sun (Member, IEEE) received the B.S. degree in computer science and technology, the M.S. degree in computer application, and the Ph.D. degree in control theory and control engineering from Nankai University, Tianjin, China, in 2003, 2006, and 2009, respectively.

Since 2009, she has been a Lecturer with the Institute of Robotics and Automatic Information System, Nankai University. Her research interests are in micromanipulator, image processing, and computer vision.